(S1A)

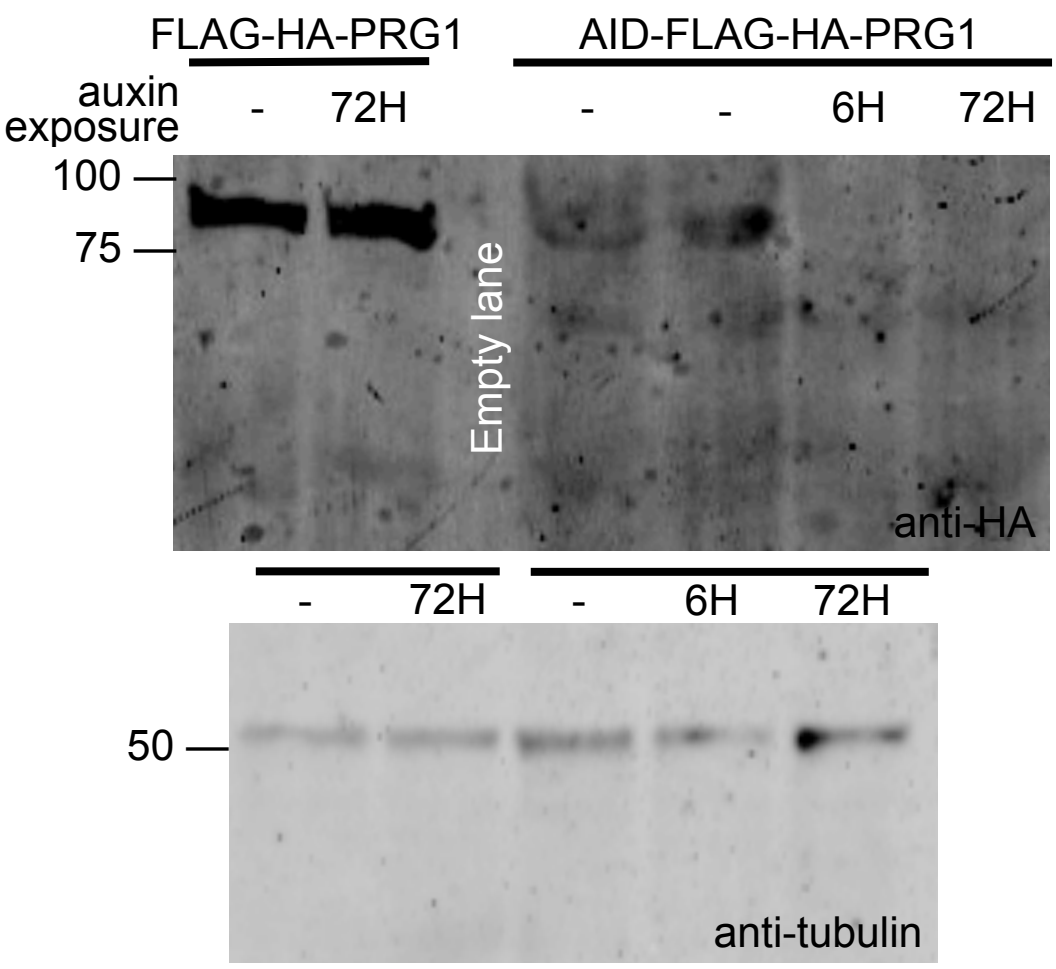

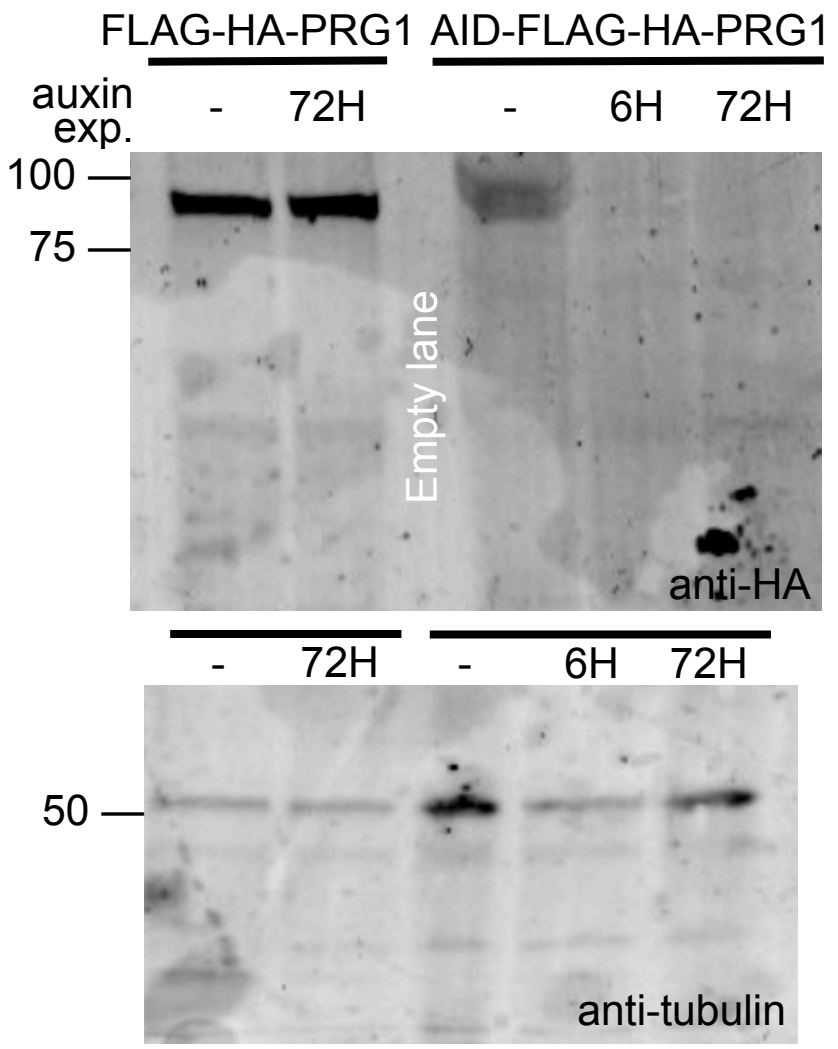

(S1B)

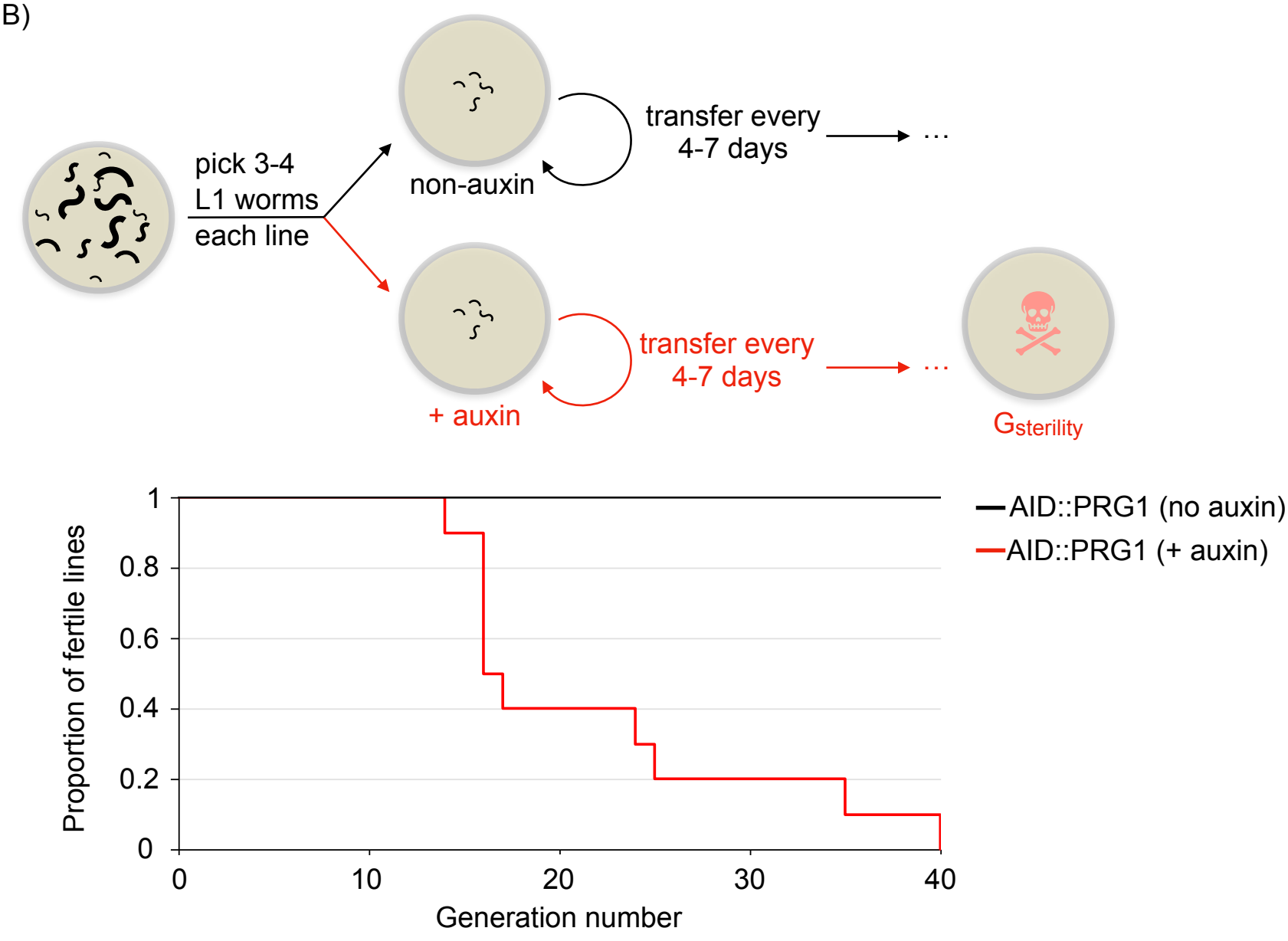

Figure S1. AID-mediated depletion of PRG-1 phenocopies the mortal germline phenotype of *prg-1(-),* Related to Figure 1. (A) Demonstration of AID-mediated depletion of PRG-1. *Left panel.* Full panel of western blots in Figure 1A. *Right panel*. Western blot from a second independent experiment, using antibodies against HA and tubulin. *Top panel.* Schematic of the fertility assay. Successive generations of *AID-FLAG-HA::prg-1* animals were picked on auxin-free or 1mM auxin plates till complete sterility. *Bottom panel.* Kaplan-Meier plot for lines grown on auxin-free plates (black line) or re-exposed to auxin (red line). Statistics: Log-rank test (****p <.001*, n=10 each).

(S2A)

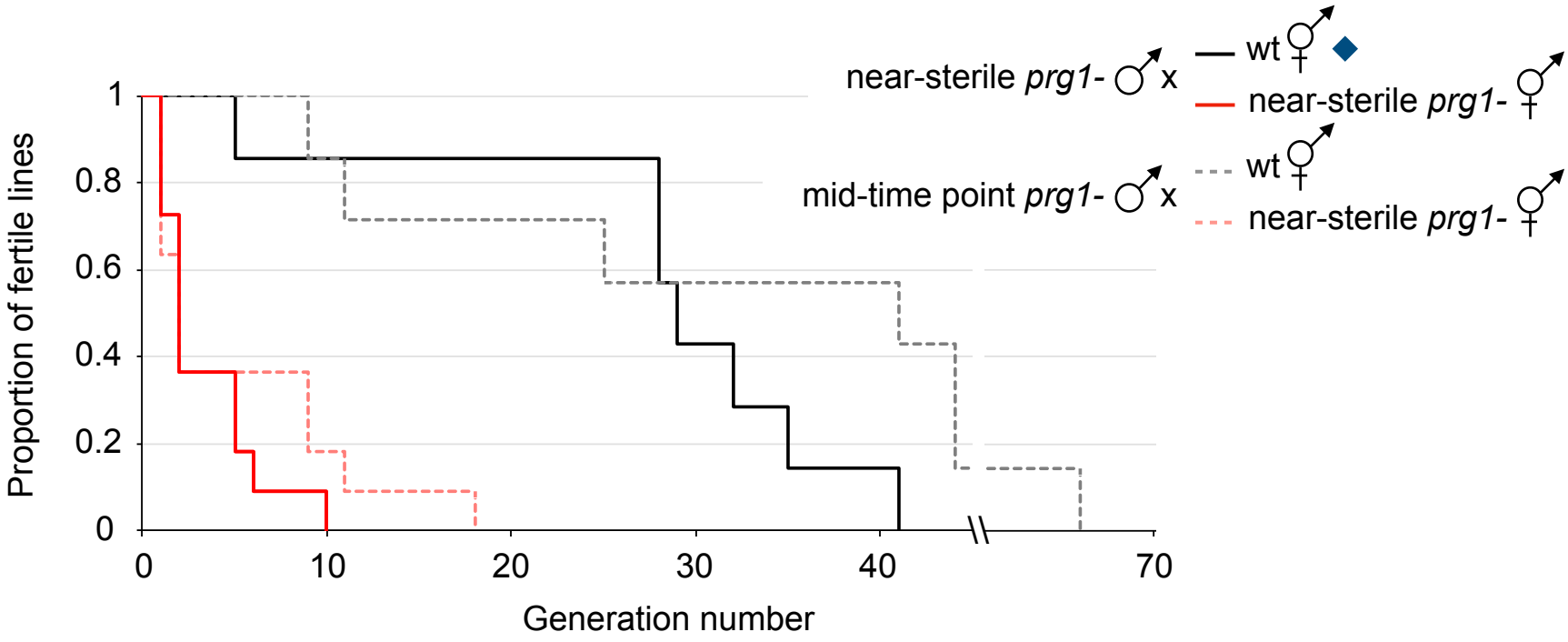
near-sterile prg1- ♂ x
wt ♀
near-sterile prg1- ♀
mid-time point prg1- ♂ x
wt ♀
near-sterile prg1- ♀
Proportion of fertile lines
1
0.8
0.6
0.4
0.2
0
0
10
20
30
40
70
Generation number

(S2B)

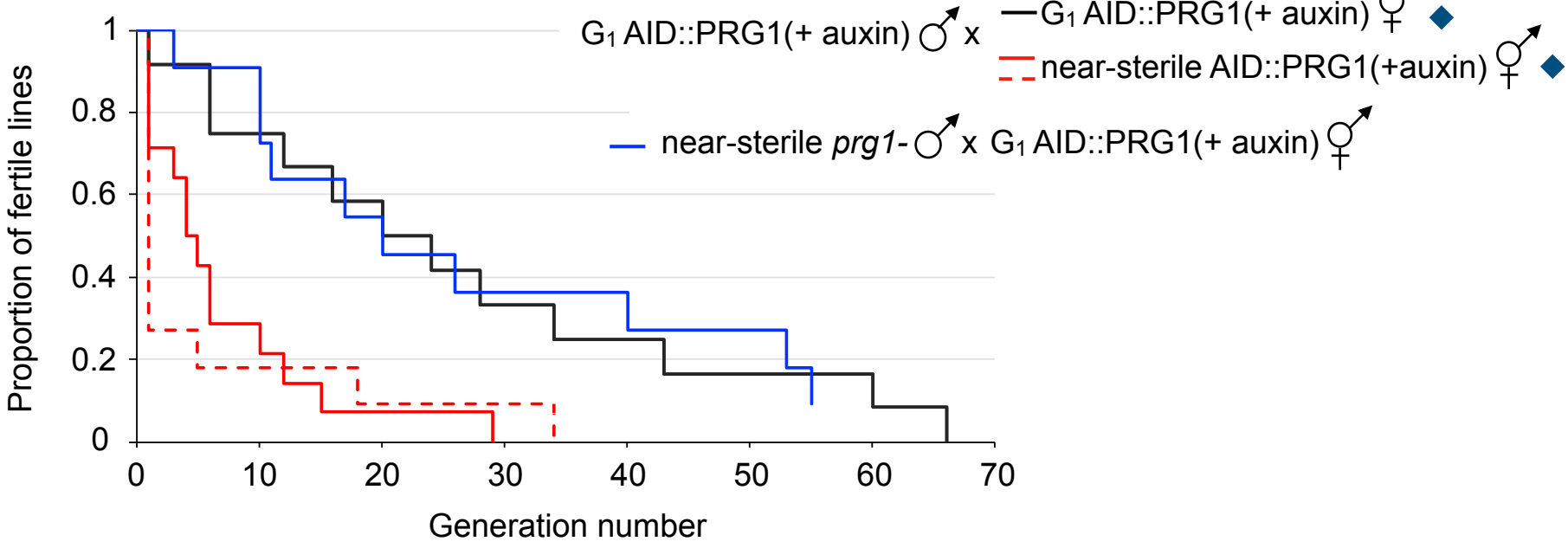
G1 AID::PRG1(+ auxin) ♂ x
G1 AID::PRG1(+ auxin) ♀
near-sterile AID::PRG1(+auxin) ♀
near-sterile prg1- ♂ x G1 AID::PRG1(+ auxin) ♀
Proportion of fertile lines
1
0.8
0.6
0.4
0.2
0
0
10
20
30
40
50
60
70
Generation number

(S2C)

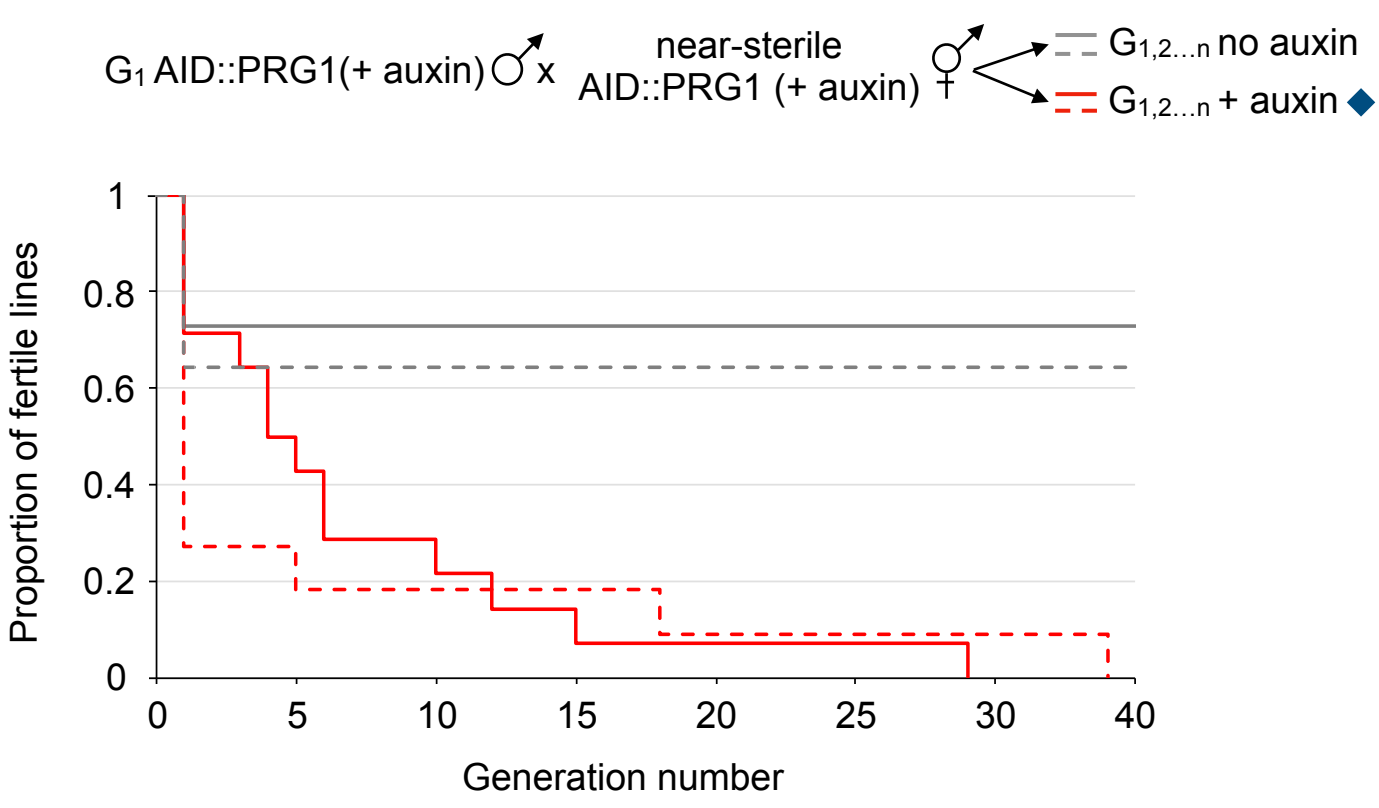
G1 AID::PRG1(+ auxin) ♂ x
near-sterile
AID::PRG1 (+ auxin) ♀
G1,2...n no auxin
G1,2...n + auxin
Proportion of fertile lines
1
0.8
0.6
0.4
0.2
0
0
5
10
15
20
25
30
40
Generation number

Figure S2. The generational age of the PRG-1(-) ooplasm is a stronger determinant of germline mortality than the age of the transferred sperm content, Related to Figure 2. (A) The effects of transferring wildtype or near-sterile ooplasm to near-sterile and mid-time point *prg-1(-)* lineages. Kaplan-Meier plot showing the proportion of fertile lines across generations for progeny from near-sterile *prg-1(-)* males crossed to near-sterile *prg-1(-)* hermaphrodites (solid red line, n=11), and progeny of mid-time point *prg-1(-)* males crossed to wildtype (hatched black line, n=7) or near-sterile *prg-1(-)* (hatched red line, n=11) hermaphrodites. Data for near-sterile *prg-1(-)* males crossed to wildtype hermaphrodites is also in Figure 2A (solid black line, and denoted with blue diamond). Note that the reset of transgenerational sterility was not due to the cross; near-sterile *prg-1(-)* males crossed to feminized animals yield only 1-2 progeny (data not shown, and Wang and Reinke, 2008). (B) Kaplan-Meier plot showing the effect of transferring ooplasm from a first generation PRG-1(-) lineage to a near-sterile *prg-1(-)* (blue line, n=11). All other lines as in Figure 2B (denoted with blue diamond). (C) Following the transfer of ooplasm from a near-sterile *prg-1(-)* lineage to a first generation auxin-treated PRG-1(-) lineage, a subset of lines were subsequently propagated on non-auxin plates, restoring PRG-1 expression (grey lines, 2 independent experiments, n=12 for both). Other lines as in Figure 2B (denoted with blue diamond).

(S3A)

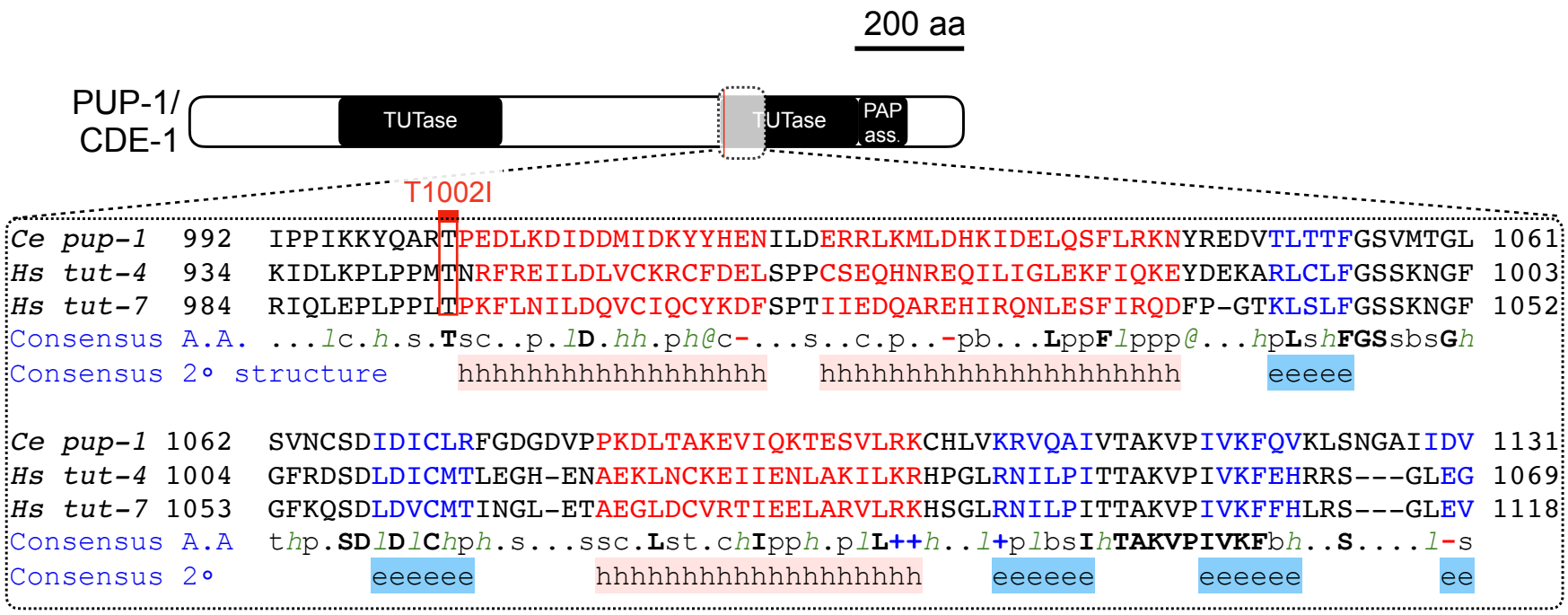

Consensus amino acid symbols:

conserved: **bold and uppercase** letters (such as **G**);

aliphatic residues (**I, V, L**): *l*

aromatic residues (**Y, H, W, F**): @

hydrophobic residues (**W, F, Y, M, L, I, V, A, C, T, H**): *h*

alcohol residues (**S, T**): o

polar residues (**D, E, H, K, N, Q, R, S, T**): p

tiny residues (**A, G, C, S**): t

small residues (**A, G, C, S, V, N, D, T, P**): s

bulky residues (**E, F, I, K, L, M, Q, R, W, Y**): b

positively charged residues (**K, R, H**): +

negatively charged residues (**D, E**): -

charged (**D, E, K, R, H**): c

Consensus secondary structure prediction symbols:

alpha-helix: h **beta-strand**: e

(S3B)

Figure S3. Suppressor mutations in the polyuridylation enzymes, Related to Figure 3. (A) The suppressor mutation T1002I in *pup-1/ cde-1* is in a conserved residue. Protein alignments shown are *C. elegans* PUP-1/CDE-1 (residues 992 to 1131), *H. sapiens* TUT-4 (934 to 1069) and TUT-7 (984 to 1118). Alignments are done with PROMALS3D, which incorporates predicted secondary and tertiary structures to align more divergent sequences as above. (B) The intronic suppressor mutation (nucleotide position 1525) in *pup-2* alters the highly conserved 3' splice site consensus sequence. R denotes a purine (A or G) nucleotide.

(S4A)

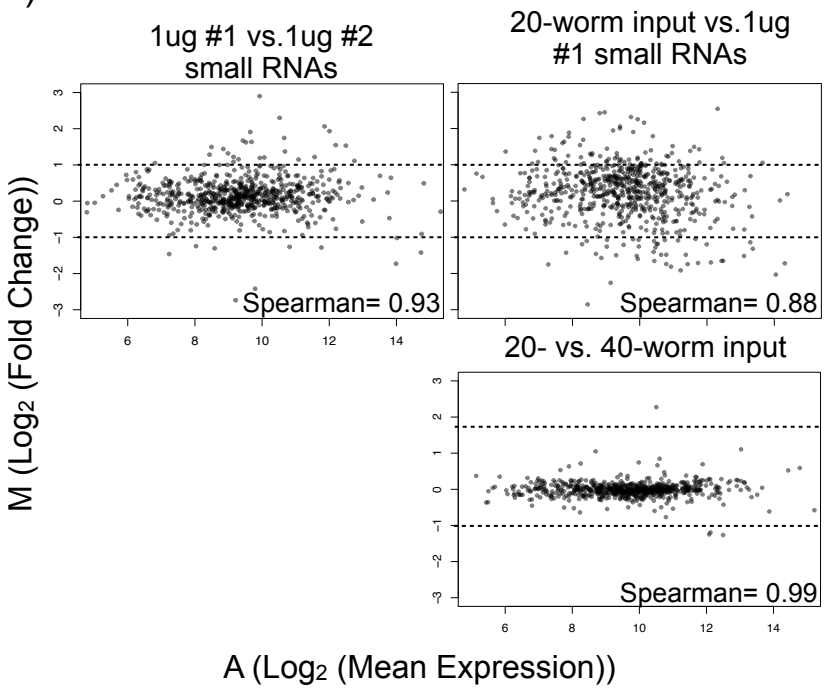

(S4B)

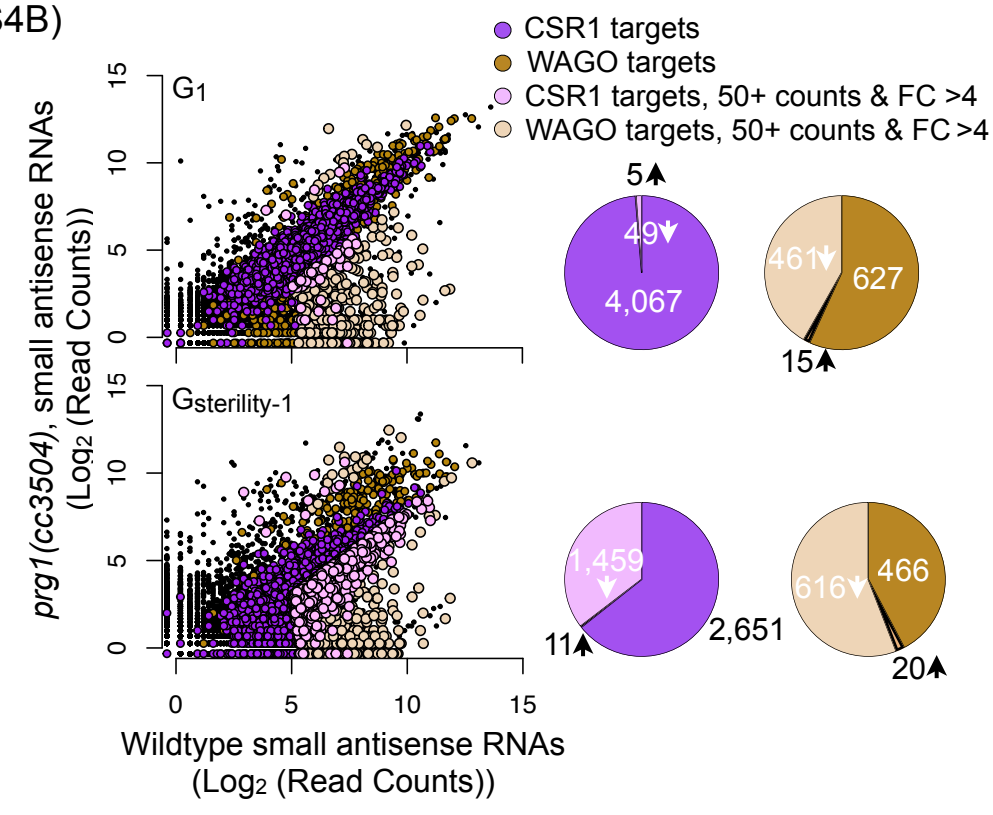

(S4C)

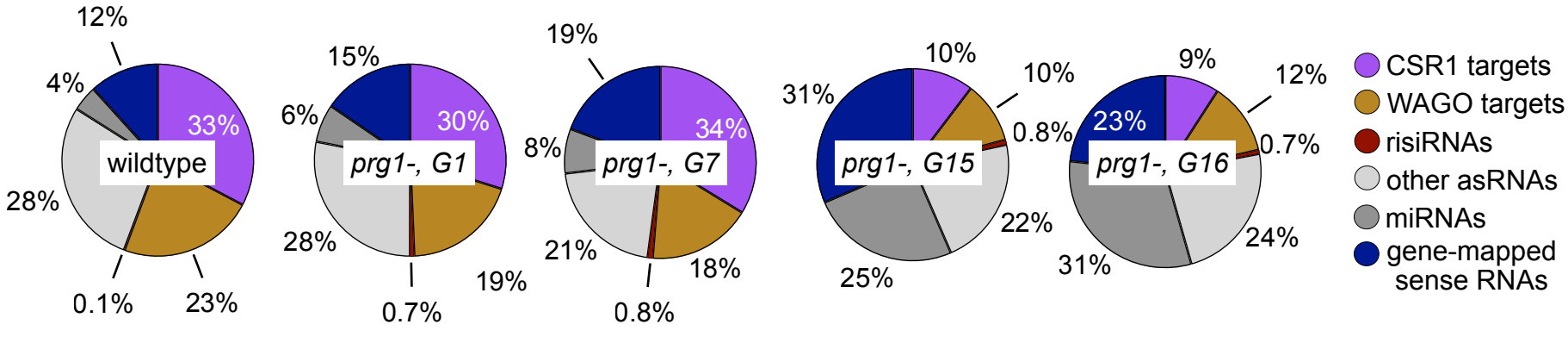

(S4D)

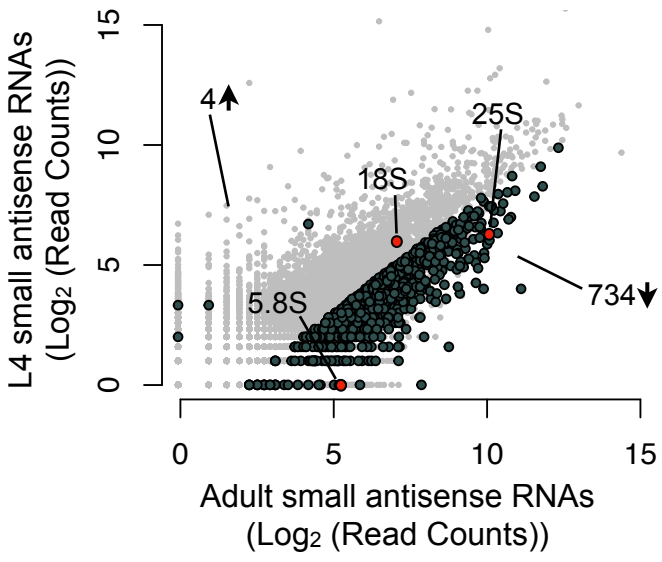

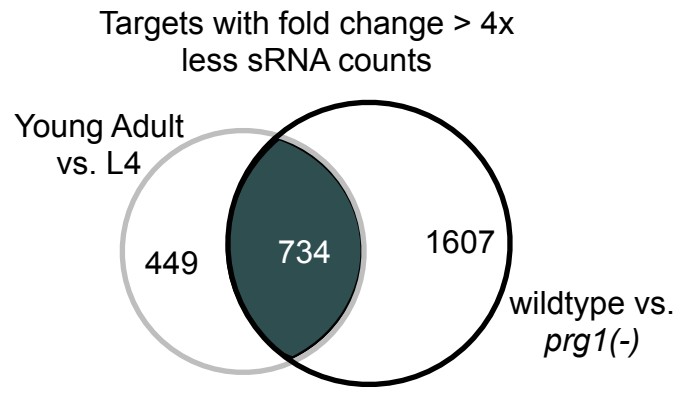

(S4E)

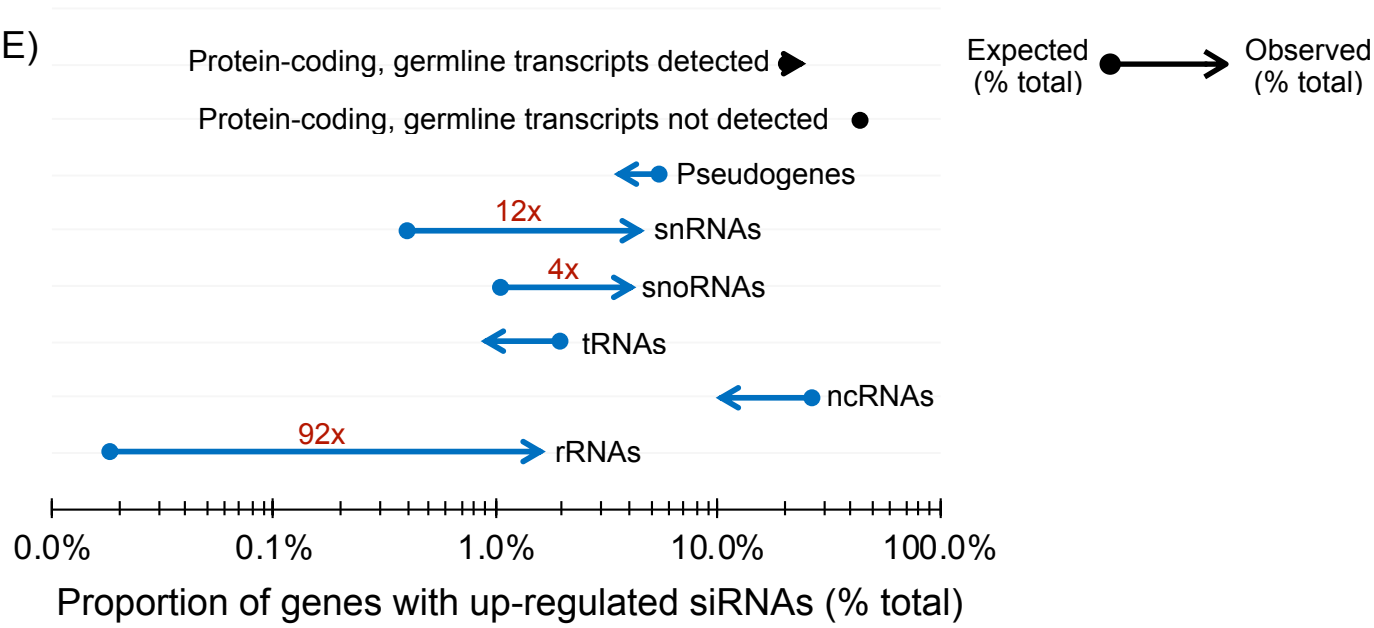

Figure S4. Classes of small RNAs with altered levels in *prg-1(-),* Related to Figure 4. (A) Similarity assessment of small RNA counts from libraries prepped with small-scale input (20 and 40 animals) versus standard input (1 ug) amounts. MA plots depict the difference in counts of small RNAs for each 150 kb bin of the *ce11* genome, per 10^6 total mapped; x-axis values are the log-transformed average count for the two input amounts, and y-axis values are log ratio of the two. (B) Overlap of genes with altered small RNA levels in *prg-1(-)* with published targets of CSR-1-bound small RNAs, and genes targeted by the WAGO pathway. Scatterplots as in Figure 3A, with CSR-1 and WAGO class gene targets indicated as dark violet and dark orange colored dots, respectively. Genes with a fold change (FC) in *prg-1(-)* that meets the criteria listed in Figure 3A, and also annotated as one of the two classes are indicated in light violet and light orange. The number of genes overlapping and non-overlapping between lists are also depicted in the pie charts right of each scatterplot. WAGO and CSR-1 small RNAs are hypothesized to surveil the germline's transcripts, helping maintain its function by regulating gene expression (Claycomb et al., 2009; Gu et al., 2009; Yigit et al., 2006). *C. elegans* piRNAs have been implicated in triggering the biogenesis of WAGO-associated small RNAs at presumptive endogenous targets through imperfect and/or partial complementarity (Lee et al., 2012; Bagijn et al., 2012). The reduced levels of WAGO-associated small RNAs in *prg-1(-)* was previously interpreted as indicating piRNA-mediated initiation of WAGO small RNAs at target loci (Bagijn et al., 2012; Lee et al., 2012; Seth et al., 2018). We note however that in late-generation *prg-1(-)* animals, the set of genes with reduced levels of small antisense RNAs are a superset of WAGO targets, with ~73% of affected genes not annotated as such (Figure S4B-C). In fact, nearly 60% of affected genes are putative CSR-1 targets, not posited to be direct targets of PRG-1. The reductions in small RNA levels (both for WAGO and non-WAGO targets) in the absence of piRNAs point to at least a subset being an indirect consequence of the progressive change in germline architecture and developmental delays associated with the partial to full sterility of *prg-1(-)*. Three additional pieces of data support this view. First, a change in germline size and architecture in *prg-1(-)* adults, even from fertile generations, has been reported previously by Heestand et al. (2018) and confirmed from our observations. The representation of WAGO-associated small RNAs in libraries may be particularly affected by differences in the cellular composition that occur upon passage of *prg-1* mutant strains. In particular, WAGO-associated small RNAs appear to be preferentially expressed in mature gametes (Reed et al., 2020), the cell types most depleted in the germlines of *prg-1(-)* animals (Heestand et al., 2018). Second, we find that nearly a third of small RNAs depleted in near-sterile *prg-1(-)* animals coincide with developmentally regulated small RNAs that are upregulated in wildtype young adult animals relative to the developmentally earlier L4 larval stage (Figure S3D). Mature sperm are present at the L4 stage, and mature oocytes develop after, during adulthood. Hence observed small RNA changes in L4 vs. adult animals may in part be due to the absence of oocytes. Additionally, observed changes may result from more deliberate developmental regulation of these small RNAs. In either case, the overlap of a subset of development-dependent small RNAs with those depleted in young adult *prg-1(-)* animals may be indicative of developmental delays relative to wildtype, as the development stage in published studies (as well as ours) are defined by timing rather than specific morphological features. Finally, only ~7% of the loci identified as having reduced levels of small RNAs in near-sterile *prg-1(-)* whole animal libraries also met the cutoff criteria listed above in libraries from dissected gonads (Figure S5B,C). Collectively these data indicate that the small RNA changes identified in whole animals may be confounded by cellular composition differences between wildtype and mutant. (C) Distribution of reads matching the indicated class of small RNAs in the various small RNA libraries. (D) *(Left)* Scatterplot depicts antisense small RNAs per gene in wildtype animals in the fourth larval (L4) stage relative to young adults (data from Maniar and Fire, 2011). Genes with a fold change meeting the criteria listed in Figure 3A in L4 stage relative to young adult animals were identified, and those with overlap to mis-regulated genes in $G_{sterility\text{-}1}$ *prg-1(-)* are indicated in dark cyan. Red dots indicate small RNA levels against the three genes in the 45S ribosomal locus (18S, 5.8S and 25S). *(Right)* Venn diagram depicting the number of genes with small RNAs reduced by at least 4-fold overlapping and non-overlapping between the lists. (E) Enrichment of genes with upregulated small RNAs among various transcript categories. The fold enrichment for over-represented categories is indicated.

(S5A)

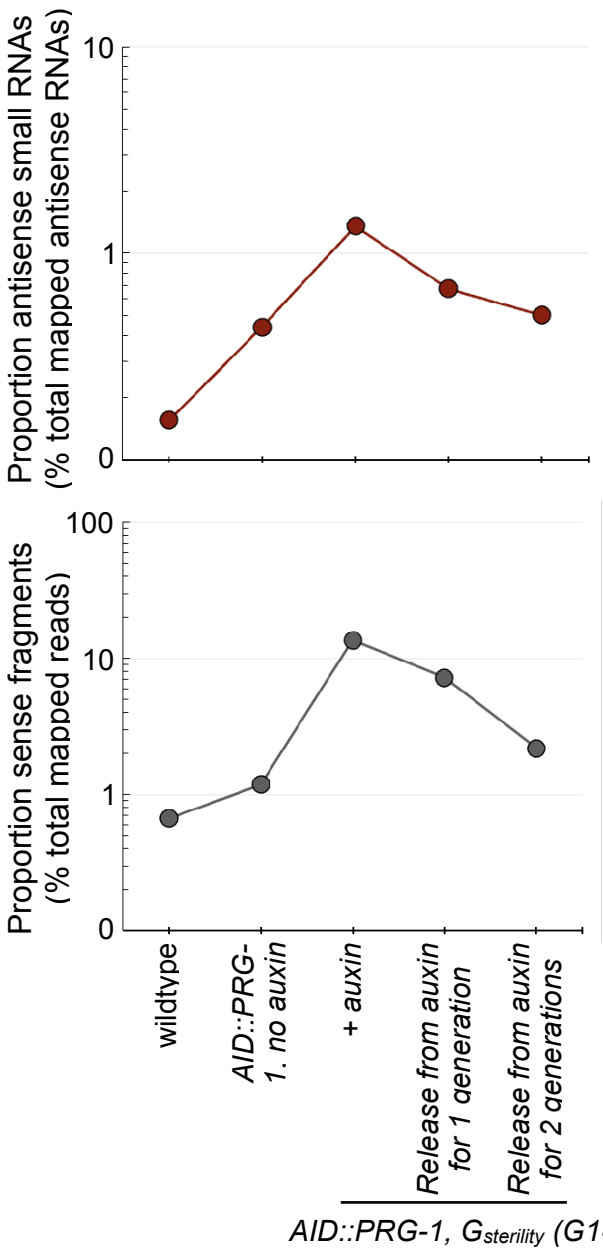

(S5B)

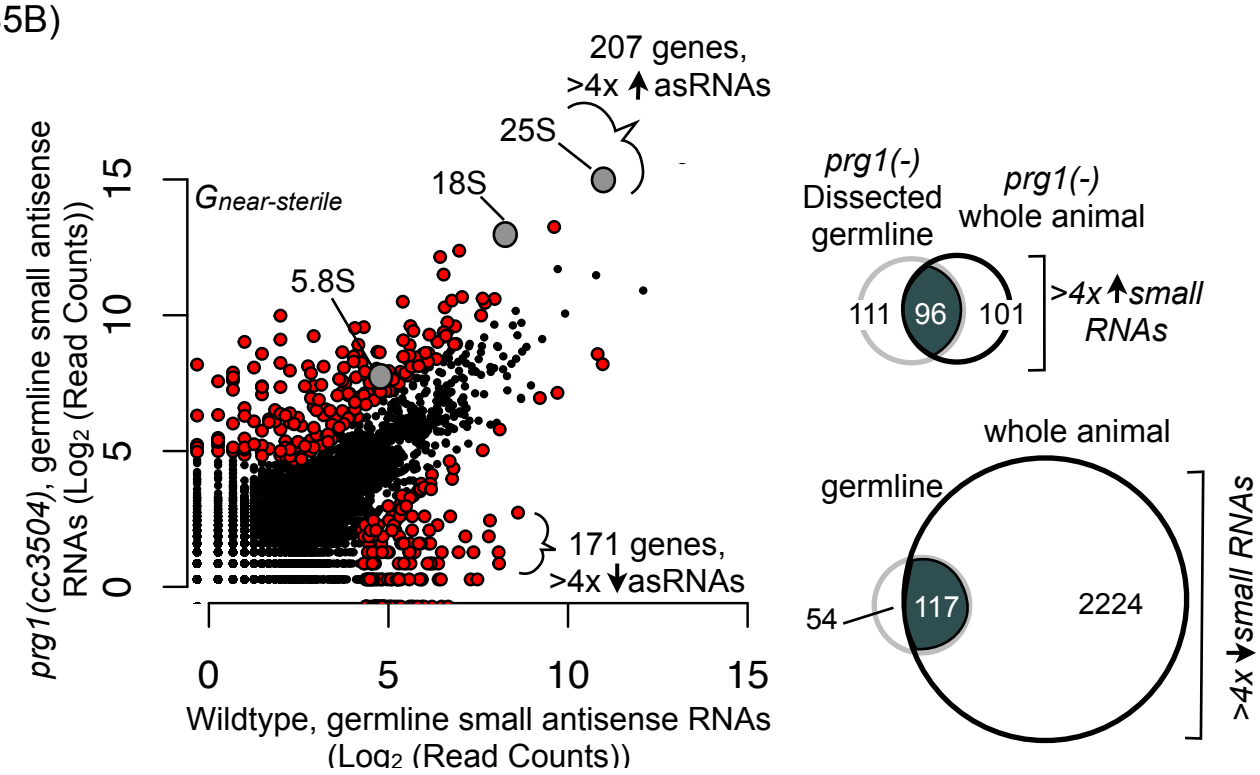

(S5C)

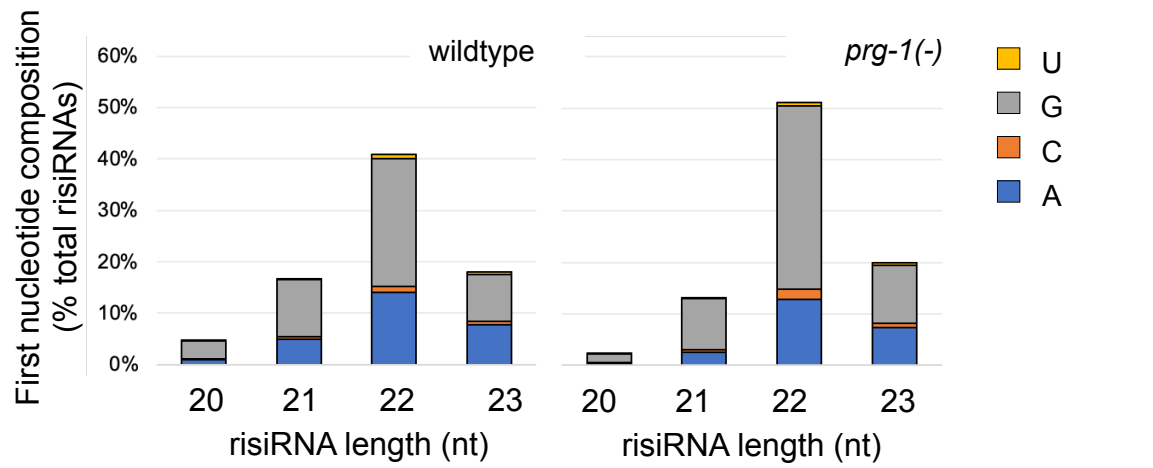

(S5D)

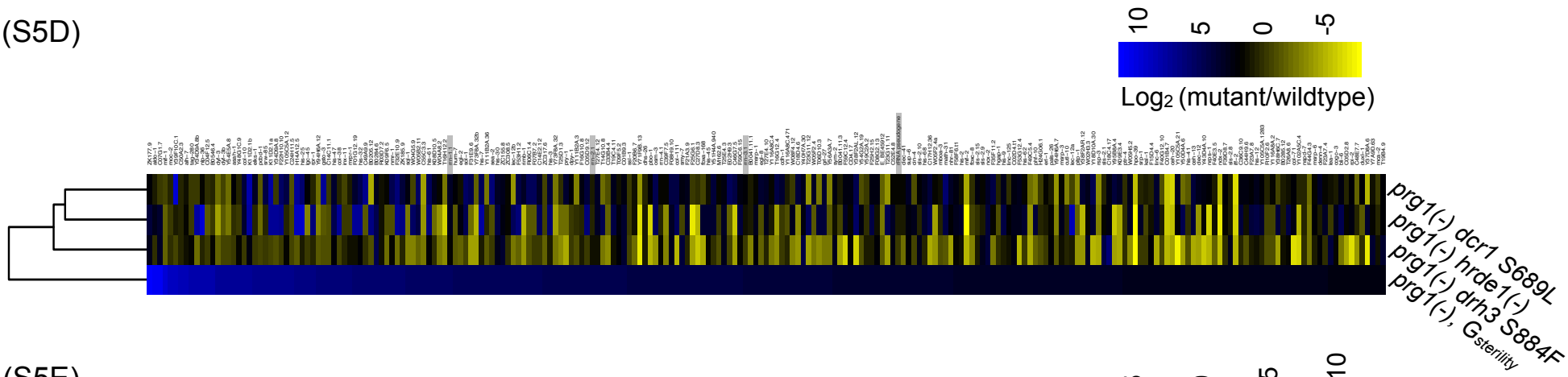

(S5E)

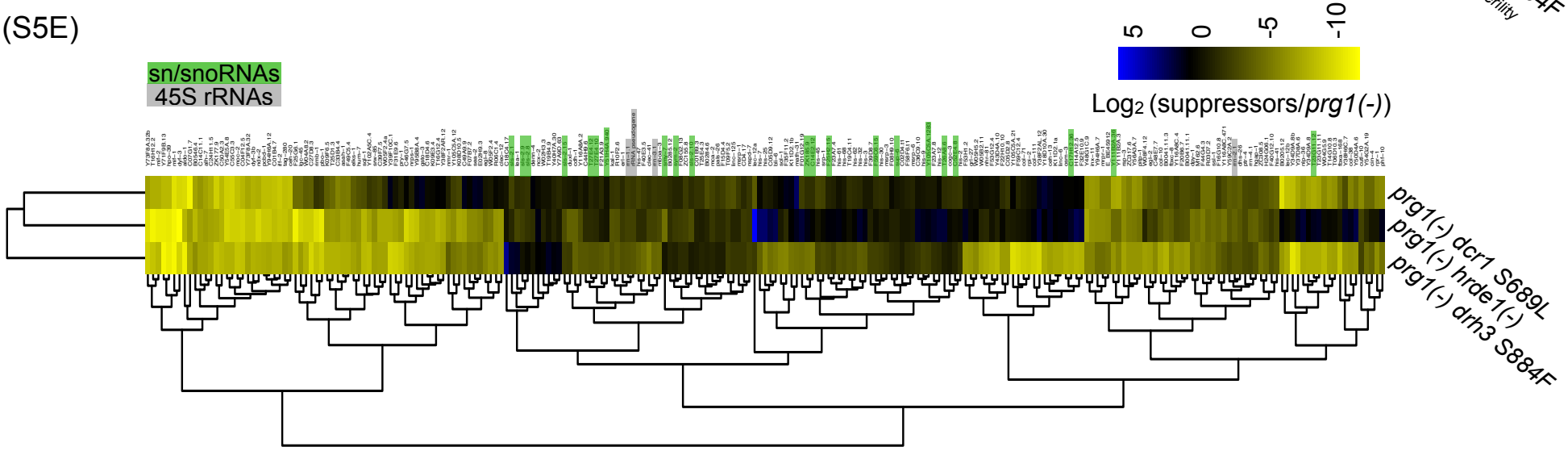

(S5F)

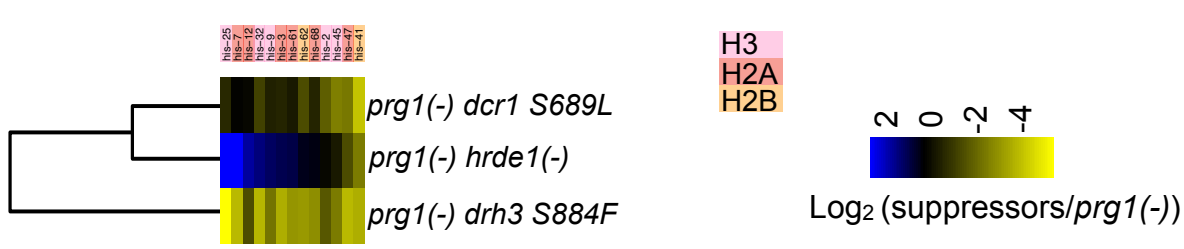

Figure S5. small RNAs hyper-accumulated in the *prg-1(-)* mutant and the effect of suppressors of the transgenerational sterility phenotype, Related to Figure 5. (A) (*Top)* Proportion of risiRNAs in AID::PRG-1 animals in the absence and presence of auxin, and for the two generations following release from auxin-mediated degradation. Values are percent of total mapped antisense RNAs. *(Bottom)* Proportion of small RNA library mapped in the sense orientation to the 45S ribosomal locus, represented as a proportion of total mapped RNAs. (B) *(Left)* Scatterplot depicts antisense small RNAs per gene in young adult near-sterile *prg-1(-)* animals relative to small RNAs per gene in wildtype animals. Counts are per 10^6 reads mapped to the ce11 genome, and represent the mean of two biological replicates. Red colored dots indicate genes meeting the three criteria listed in Figure 3A, and the grey dots denote the three genes in the 45S ribosomal locus (18S, 5.8S and 25S). *(Right)* Venn diagrams depicting the number of genes with small RNAs increased or reduced by at least 4-fold overlapping and non-overlapping between libraries from dissected germline and whole animal. (C) Start nucleotide and size distribution of risiRNAs. (D) Change in small RNA reads in *prg-1(-)* animals and suppressors. Heatmap depicts the log-transformed fold change in small RNA read counts mapped to listed genes in adult animals from $G_{sterility}$ *prg-1(-)*, *prg-1(-);dcr-1*[S689L], *prg-1(-);drh-3*[S884F] and *prg-1(-);hrde-1(-)* relative to wildtype. All read count values are normalized to total mapped reads, and represent the mean of two biological replicates. Genes included here have > 4-fold increase in small RNAs in $G_{sterility}$ *prg-1(-)* animals and meet the fold change criteria introduced in Figure 4A (n=235). Fold changes are relative to wildtype and genes are ordered in descending order of the fold change in $G_{sterility}$ *prg-1(-)*. (E) Heatmap and hierarchical clustering depicting the log-transformed fold change in small RNA reads for the *prg-1(-);dcr-1*[S689L], *prg-1(-);drh-3*[S884F] and *prg-1(-);hrde-1(-)* relative to $G_{sterility}$ *prg-1(-)*. Column and row dendrograms indicate the similarity between the changes in strains and genes, respectively. Genes coding for snRNA/snoRNAs and 45S rRNA genes are indicated. (F) Heatmap as in Figure S5E depicting the changes in small RNAs mapped to histone-coding genes. The family of histones each gene belongs to is indicated.

(S6A)

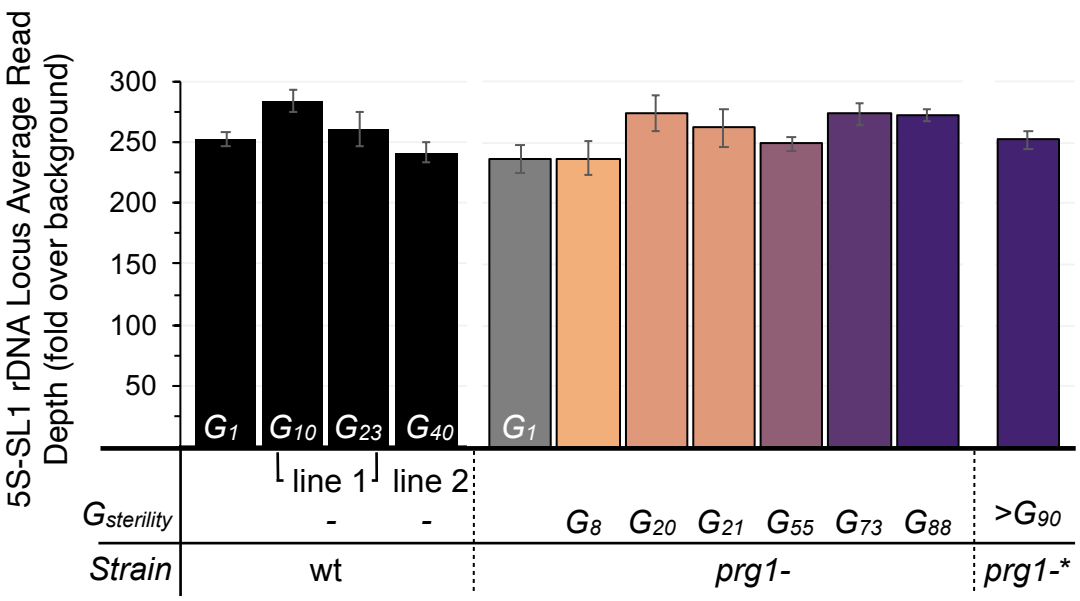

(S6B)

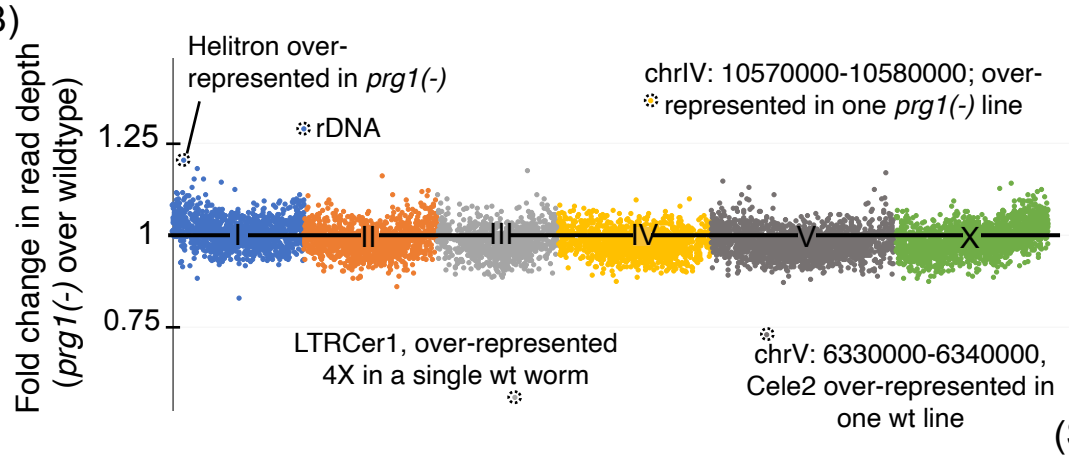

(S6C)

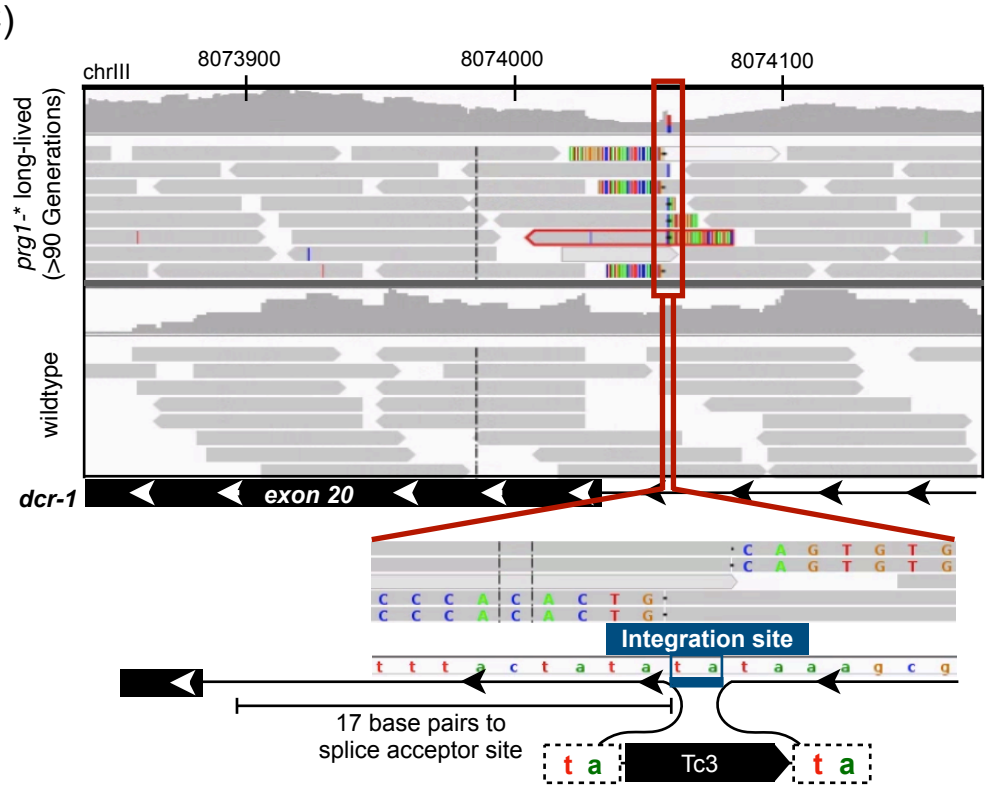

(S6D)

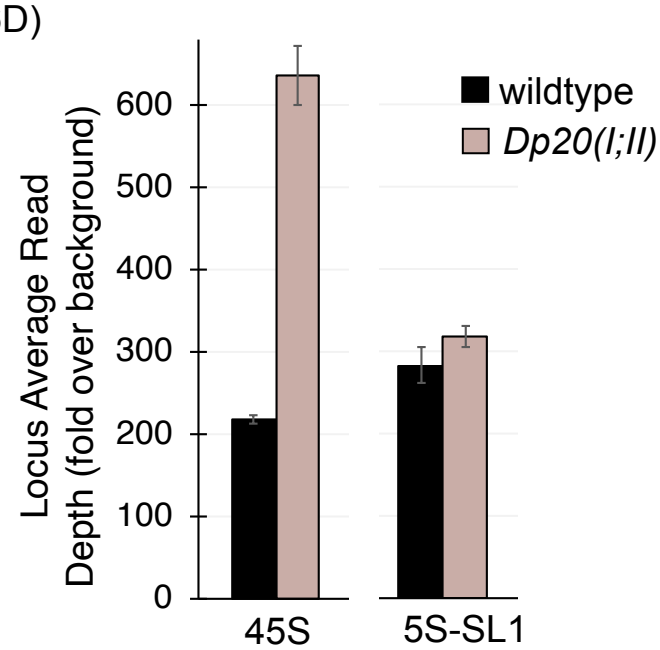

(S6E)

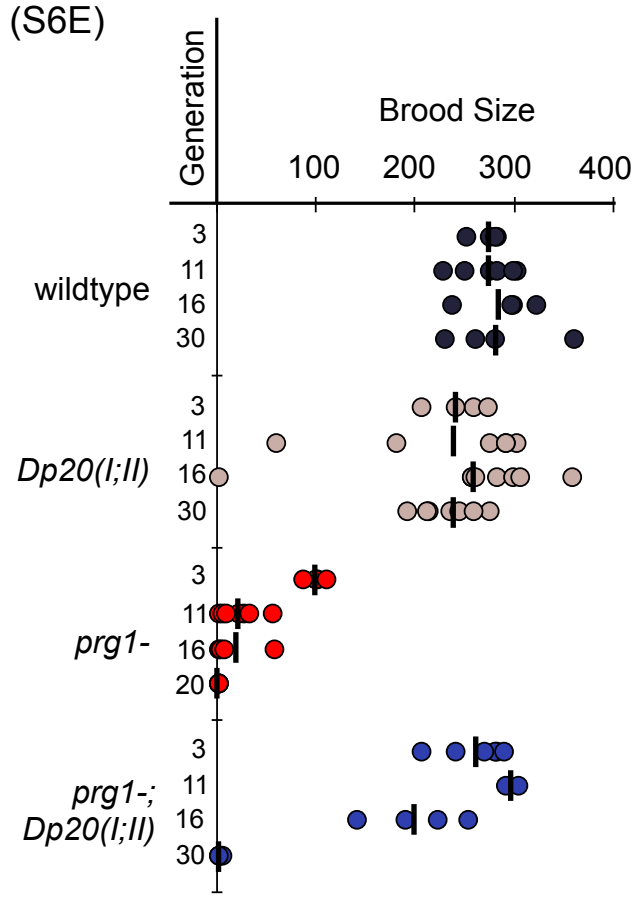

(S6F)

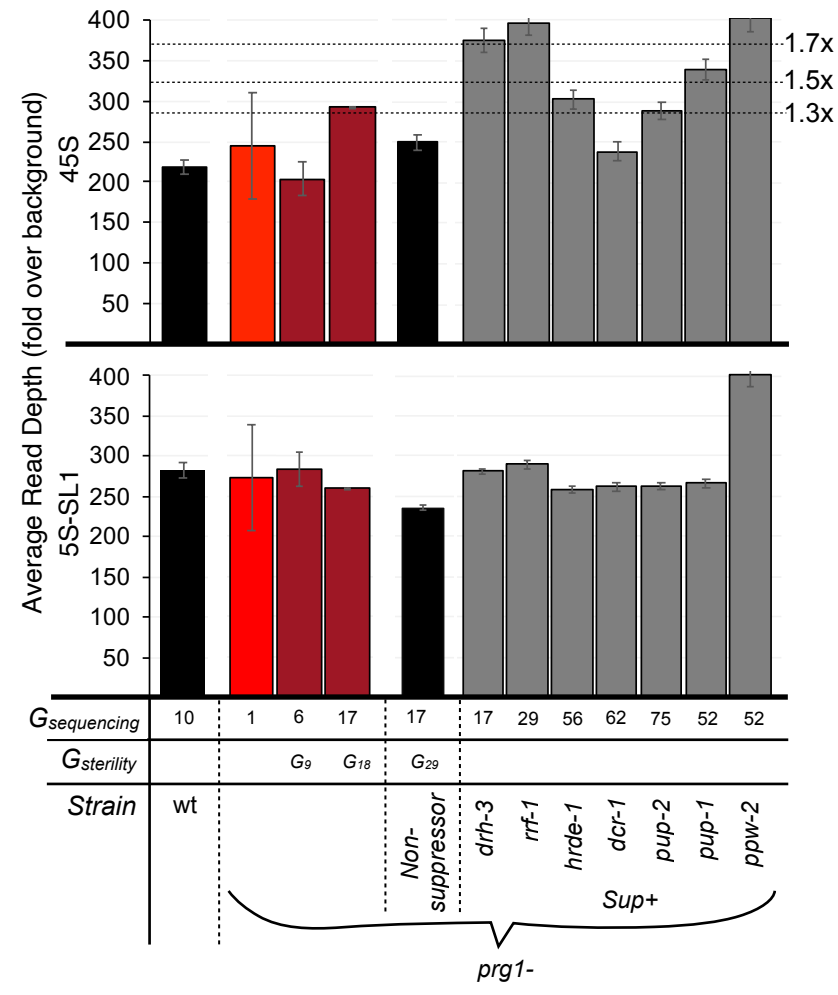

(S6G)

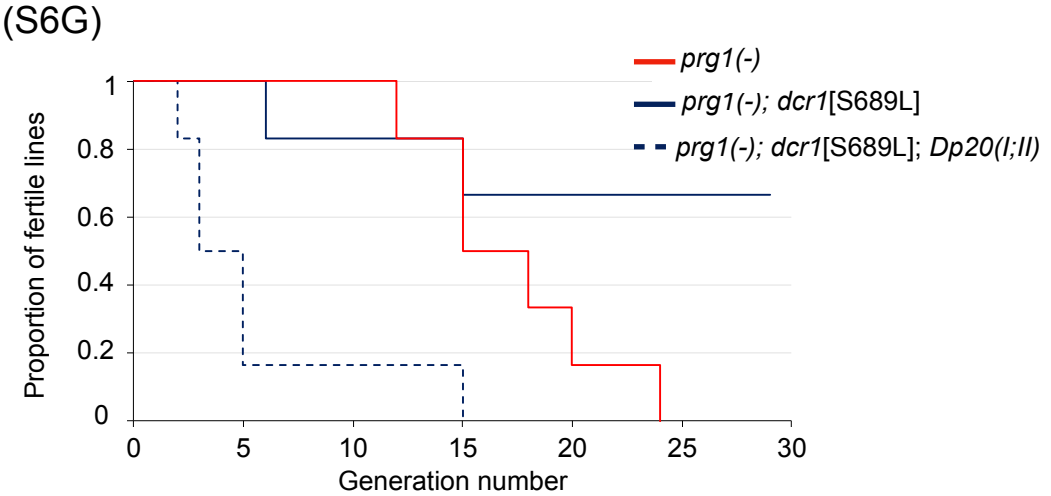

Figure S6. rDNA copy number increases correlate with a longer transgenerational lifespan in *prg-1(-)* and a subset of *prg-1(-); sup(+)* double mutants, Related to Figure 6. (A) Relative copy number of the 5S-SL1 rDNA locus in wildtype and *prg-1(-)* animals. Values represent mean read depths across the locus relative to genome-wide obtained from single-worm genome sequencing (n=3-5 animals each). Error bars represent standard error of the mean. (B) Genome-wide read coverage for *prg-1(-)* animals relative to wildtype. The *ce11* genome is divided into 10kb bins, and the normalized read depth per bin across all *prg-1(-)* animals is represented as a fold change over the normalized read depth in wildtype animals. (C) Integrated Genome Viewer snapshot of the *dcr-1* locus in the long-lived *prg-1(-)** in Figure 6A. Analysis of reads mapped to the region supported the presence of a homozygous Tc3 insertion 17 base pairs from the 20th exon's splice acceptor site. *Dcr-1* is coded by a total of 26 exons. We manually inspected and verified that no additional variants were detectable at the other six suppressor loci recovered in the screen. (D) Validation of increased copy number in *eDp20(I;II)* Relative copy number of the 45S rDNA locus and 5S-SL1 rDNA locus in wildtype, *prg-1(-)* and *prg-1(-); suppressor(+)* doubles. (E) Increasing the copy number of the 45S locus does not significantly change the brood size of *prg-1(+)* animals. Brood size assays quantifying the number of progeny produced over the worm's reproductive lifetime in the indicated genotypes and generations after the start of the fertility assay. Each dot represents broods from individual animals, and the black bar indicates the mean of them (n=4 to 6). (F) Relative copy number of the 45S rDNA locus *(Top panel)* and 5S-SL1 rDNA locus *(Bottom panel)* in wildtype, *prg-1(-)* and *prg-1(-); suppressor(+)* doubles. Values represent mean read depths across the rDNA loci relative to genome-wide obtained from genome sequencing of bulk populations. For each sample four separate PCR reactions are done, and error bars represent standard error of mean for the reactions. For each strain, the generation at which sequencing was done, as well as that of sterility are indicated. All suppressor strains were maintained to at least G_{100}. (G) Proportion of fertile *prg-1(-);dcr-1*[S689L] lines with additional rDNA copies introduced. Kaplan-Meier plot for *prg-1(-);dcr-1*[S689L] animals with (blue hatched line, n=6) and without (blue solid line, n=6) a duplication of the 45S rDNA locus (*Dp20(I;II))*, and control *prg-1(-)* (red line, n=6). Statistics: Log-rank test (****p <.001* for *prg-1(-);dcr-1*[S689L] and *prg-1(-);dcr-1*[S689L]*;Dp20(I;II),*).

(S7A)

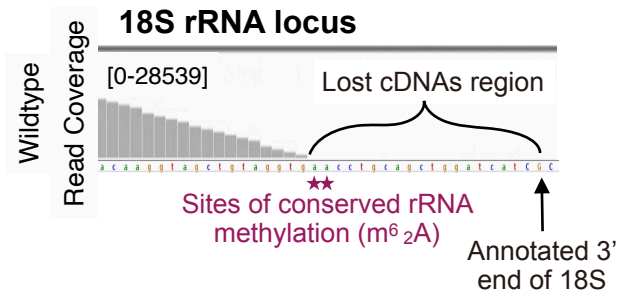

(S7B)

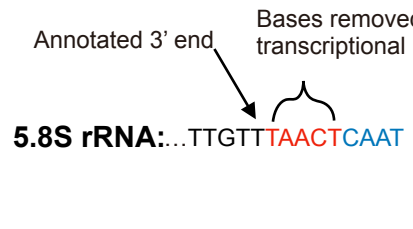

Captured 3' ends	wt	near-sterile *prg-1(-)*
...TTG	3.21%	2.91%
...TTGT	4.85%	4.39%
...TTGTT	9.78%	9.76%
...TTGTTT	71.3%	74.9%
...TTGTTTA	1.57%	0.99%
...TTGTTTAA	1.73%	0.90%
...TTGTTTAAC	1.51%	1.01%
...TTGTTTAACT	0.35%	0.25%
...TTGTTTT	0.02%	0.02%
...TTGTTTTT+	0.01%	0.01%
...TTGTTTAACTT	0.04%	0.03%

Annotated 3' end
26S rRNA:...TTTGTTTC

Captured 3' ends	wt	near-sterile *prg-1(-)*
...TTTG	15.2%	16.9%
...TTTGT	81.8%	79.9%
...TTTGTT	0.52%	0.48%
...TTTGTTT	0.1%	0.05%
...TTTGTTTT+	0.05%	0.005%

(S7C)

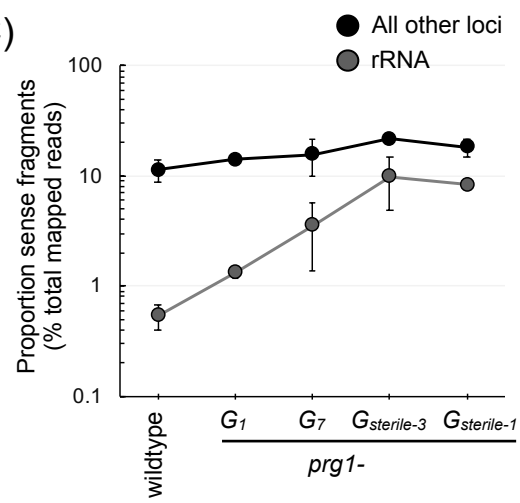

(S7D)

	sense rRNA fragments (per 10^6 mapped)	Reads with untemplated base additions (% total sense fragments)	Untemplated base(s) added (% total sense fragments)			
			U	UU	UUU	4U+
wildtype	33222 (±4450)	3.80 (±0.37)	0.53 (±0.06)	0.021 (±0.003)	0.005 (±0.001)	0.006 (±0.002)
prg1-, sterile generation	193002 (±29850)	5.08 (±0.35)	0.93 (±0.18)	0.21 (±0.02)	0.06 (±0.0001)	0.086 (±0.002)
p-value	*.00E0*	*1.25E-15*	*2.05E-13*	*3.44E-18*	*3.74E-6*	*4.62E-8*

	risiRNAs (per 10^6 mapped)	Reads with untemplated base additions (% total risiRNAs)	Untemplated base(s) added (% total risiRNAs)			
			U	UU	UUU	4U+
wildtype	3826 (±18)	21.90 (±2.82)	11.10 (±2.04)	4.65 (±0.53)	1.98 (±0.12)	2.03 (±0.06)
prg1-, sterile generation	67608 (±4731)	13.68 (±2.76)	5.83 (±1.09)	2.28 (±0.7)	0.95 (±0.31)	1.31 (±0.28)
p-value	*.00E0*	*6.03E-90*	*4.61E-76*	*3.27E-47*	*1.05E-18*	*1.34E-7*

(S7E)

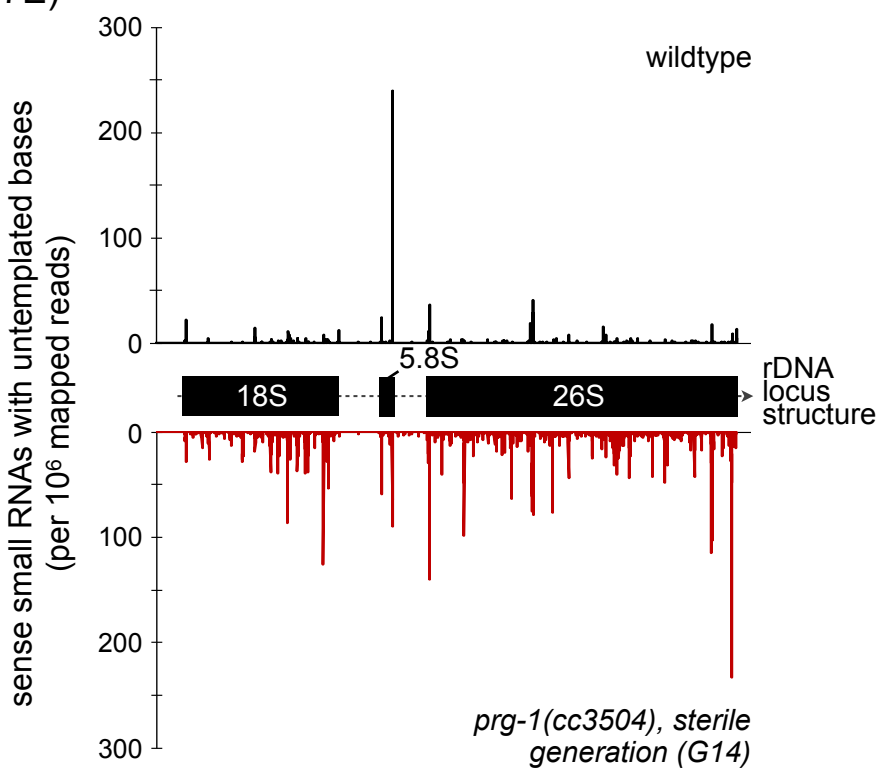

(S7F)

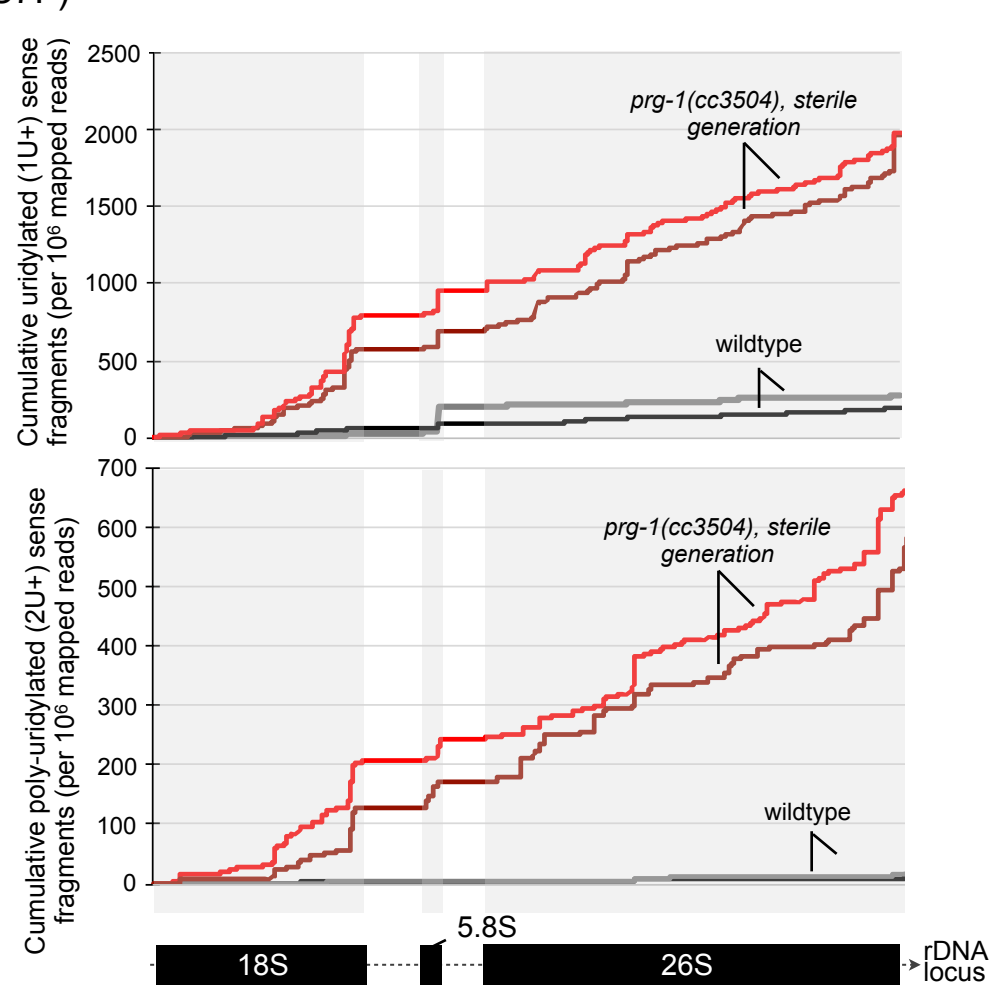

Figure S7. *prg-1(-)* animals accumulate sense rRNA fragments with untemplated 3' tail uridylation, Related to Figure 7. (A) Read coverage near the annotated 3' end of full length 18S rRNA. Integrated Genome Viewer snapshot showing the absence of coverage across the last 20 base pairs of the 18S transcript. Detectable read ends correspond to the site of two prevalent rRNA modifications upstream of the annotated 3' end, known to impede reverse transcription (Lafontaine and Tollervey, 1995). (B) Prevalence of untemplated 3' tail uridylation for full length 5.8S and 26S rRNAs. The proportion of reads ending at sites around the annotated 3' end, along with any potentially untemplated 3' uridylation events are indicated for wildtype and near-sterile *prg-1(-)* libraries. For the 26S rRNA locus, three Ts are encoded beyond the annotated 3' end, making it difficult to determine whether their presence in the RNA is due to transcriptional run-on or untemplated addition. (C) Proportion of small RNA library mapped in the sense orientation to the 45S ribosomal locus, and all other annotated genes in wildtype and across generations in *prg-1(-)*. Values are the mean of two biological replicates, represented as a proportion of total mapped RNAs. Error bars represent standard error of the mean. (D) Distribution of sense RNA fragments with untemplated 3' base additions across the 45S rDNA locus in a wildtype (black) and near-sterile *prg-1(-)* (red) replicates. The 3' end position for each sense RNA is mapped. (E) Total counts of risiRNAs and sense RNA fragments mapped across the 45S locus and proportion of risiRNAs and sense RNA fragments with untemplated 3' bases in wildtype and near-sterile *prg-1(-)* animals. Values are the mean of two biological replicates, represented as a proportion of total reads in each category. Values in between quotes represent standard error of the mean. Statistics: Cochran-Mantel-Haenszel test. (F) Cumulative counts of rRNA sense fragments with untemplated 3' uridylation in wildtype (black and grey) and sterile-generation *prg-1(-)* replicates (dark and light red). Graphs denote the 3' end position for sense RNA fragments along the 45S locus, carrying uridine additions of any length (*top panel*) or 2+ (*bottom panel*).

(S8)

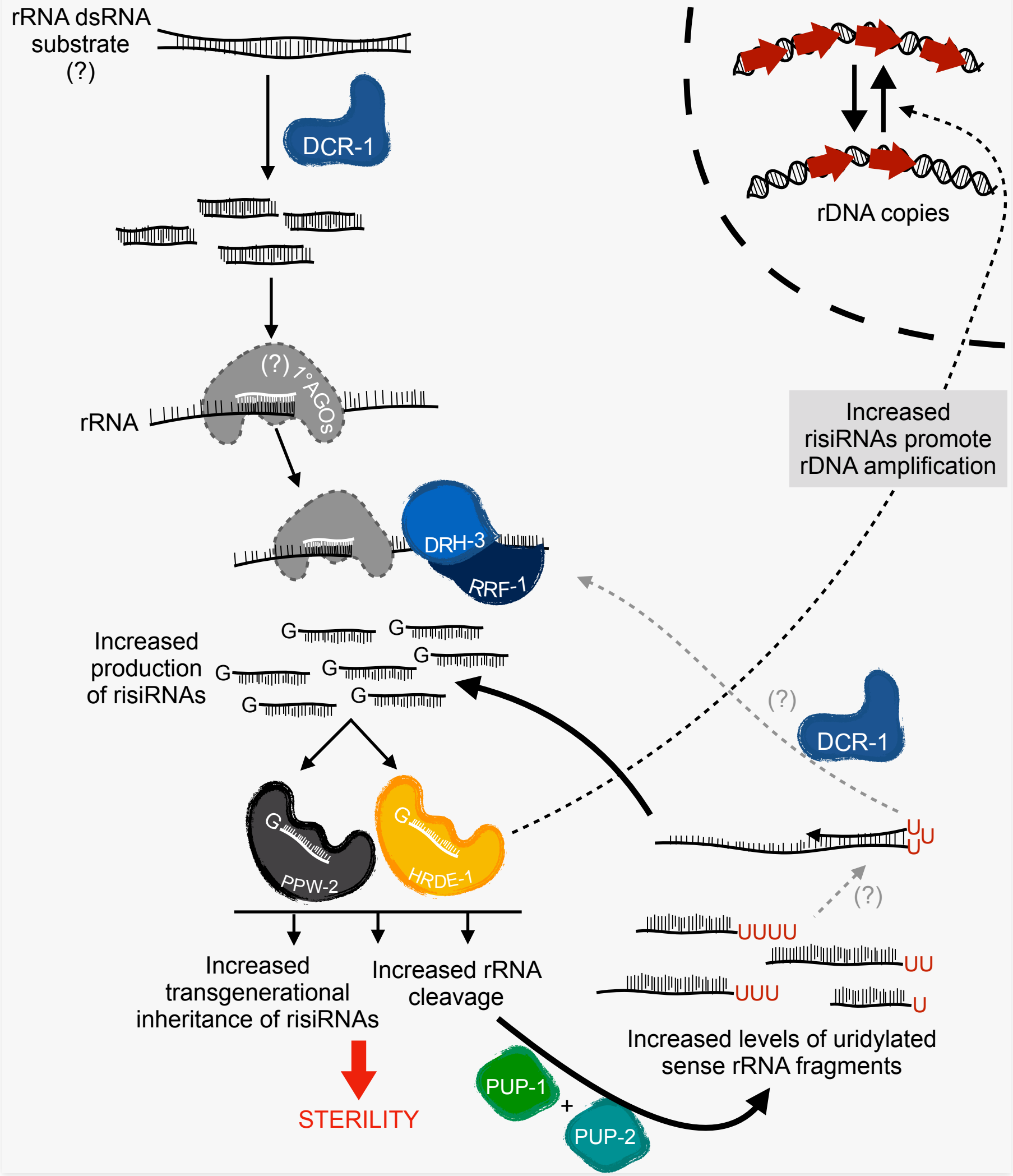

Figure S8. Model for the up-regulation of risiRNAs and rDNA copy number in *prg-1*-deficient animals, Related to Figure 7. DCR-1 may initiate risiRNA formation through processing of double-stranded rRNA molecules. Potential sources of such a double-stranded structure include: secondary structure of rRNAs, sense-antisense ds-rRNA, or an RdRP-generated ds-rRNA elongated from U-tailed sense fragments. The RdRP complex (which includes RRF-1 and DRH-3) generates the bulk of risiRNAs found in the germline, that complex with at least two WAGOs: PPW-2 and HRDE-1. These WAGOs mediate transgenerational inheritance of risiRNAs and rRNA cleavage. We posit that a consequence of rRNA cleavage is the accumulation of uridylated sense fragments; the uridylation enzymes PUP-1 and PUP-2 are involved in the transgenerational sterility phenotype of PRG-1 deficient animals, possibly through an involvement in the accumulation of risiRNAs. Finally, our data indicates that a persistent increase in risiRNA levels promotes rDNA amplification. We speculate this may result from direct interactions of the RNAi machinery with the rDNA locus. The over-production of risiRNAs triggered by the loss of PRG-1 may be due to competition for a pool of shared resources, the piRNA machinery's direct regulation of the endo-siRNA machinery, regulation of ds-rRNA trigger levels or additional yet to be discovered control mechanisms.